Research Square

Preprints are preliminary reports that have not undergone peer review.
They should not be considered conclusive, used to inform clinical practice,
or referenced by the media as validated information.

Dual-modal sensor for dopamine detection based on In 2 O 3 @FeMoSe 2 heterojunctions with excellent photoelectrochemical and peroxidase-like properties

Qing Huang
Guangxi Minzu Normal University
Ju Huang
Guangxi Minzu Normal University
Lei Huang
Guangxi Minzu Normal University
Tao Yang
Guangxi Minzu Normal University
Yanli Zhang
Guangxi University
Chendong Ling
Guangxi Huazheng New Energy Technology Co. Ltd
Cuizhong Zhang
Guangxi Minzu Normal University
Wenfeng Zhuge
zhugewf@163.com
Guangxi Minzu Normal University
Jinyun Peng
Guangxi Minzu Normal University
Qiaoqiao Sun
Guangxi Minzu Normal University

Research Article

Keywords: In2O3@FeMoSe2 heterojunctions, Dopamine, Photoelectrochemical, Colorimetric

Posted Date: November 6th, 2026

DOI: https://doi.org/10.21203/rs.3.rs-11185407/v1

License: This work is licensed under a Creative Commons Attribution 4.0 International License.
Read Full License

Additional Declarations: No competing interests reported.

Dual-modal sensor for dopamine detection based on In_2O_3@$FeMoSe_2$ heterojunctions with excellent photoelectrochemical and peroxidase-like properties

Qing Huang[1], Ju Huang[1], Lei Huang[1], Tao Yang[1], Yanli Zhang[2], Chendong Ling[3], Cuizhong Zhang [1], Wenfeng Zhuge[1], Jinyun Peng[1,2**], Qiaoqiao Sun[1]*

[1]Guangxi Key Laboratory for High-value Utilization of Manganese Resources, College of Chemistry and Materials, Guangxi Minzu Normal University, Chongzuo, 532200, Guangxi, China

[2]College of Chemistry and Chemical Engineering, Guangxi University, Nanning, 530004, China

[3]Guangxi Huazheng New Energy Technology Co. Ltd, Chongzuo, 532200, Guangxi, China

Abstract

In this work, the indium oxide and iron molybdenum selenide (In_2O_3@$FeMoSe_2$) heterojunctions were synthesized using a simple hydrothermal method. The morphological and structural properties of the obtained heterojunctions were comprehensively characterized. In-situ functionalization of the hierarchical micro-flowers of $FeMoSe_2$ with In_2O_3 nanoparticles dramatically boosts electrical conductivity, photocatalytic activity and peroxidase-like activity. Benefiting from the band gap matching of In_2O_3 and $FeMoSe_2$, and dopamine (DA) as electron donors, and realizing photocurrent signals amplification. In the presence of H_2O_2, In_2O_3@$FeMoSe_2$ catalyzes the oxidation of 3,3',5,5'-tetramethylhydrogen dioxide

* Corresponding author.

E-mail address: zhugewf@163.com (Wenfeng Zhuge)

pengjinyun@yeah.net (Jinyun Peng)

(TMB) to a blue product. DA capture hydroxyl radicals, thereby inhibiting the oxidation of TMB, which leads to a lighter blue color and a subsequent decrease in absorbance. Here, a photoelectrochemical and colorimetric dual-mode sensor for dopamine assay based on In_2O_3@$FeMoSe_2$ was constructed. The detection limits were 14.7 nM and 0.19 μM (S/N = 3), respectively. The sensor was successfully applied to the detection of dopamine (DA) in human serum and urine samples, exhibiting high sensitivity, excellent reproducibility, and reliable stability. To the best of our knowledge, this strategy for DA detection has not been previously reported.

Keywords: In_2O_3@$FeMoSe_2$ heterojunctions; Dopamine; Photoelectrochemical ; Colorimetric

1. Introduction

Dopamine (DA) is a crucial neurotransmitter in the human central nervous system known to humans that helps human cells to transmit a variety of chemicals [1]. DA concentration range in the human body is in a dynamic balance with the existence of self-regulatory mechanisms with mental stimuli . It may cause some very serious diseases, including local ischaemia, Alzheimer's disease, Parkinson's disease in children and even neuropsychiatric disorders [2-4] when DA concentrations are chronically imbalanced. Therefore, the exploration of a sensitive assay that can accurately quantify DA is crucial for and human health [5-6].

At present, several strategies such as fluorescence spectrophotometry [7], ultraviolet spectrophotometry [8], capillary electrophoresis [9], electrochemical

detection[10], photoelectrochemical (PEC) detection [11] etc. are available for the quantitation of DA. Among them, PEC sensors are believed to an innovative and promising strategy in recent years. By employing light and electrical energy forms, PEC sensors often exhibit higher sensitivity, lower background signal, shorter reaction time and lower detection limit [12]. The microsensors are simple faster detection speed and low cost. Meanwhile, colourimetric sensors are also favoured by researchers because of their visual and qualitative properties. Although both sensors have their unique advantages and characteristics, the single-signal mode is susceptible to external interference, which leading to false-positive or false-negative results and thus weak resistance to interference. In addition, single signals do not provide internal reference correction, making it difficult to ensure high accuracy and reliability of the results [13]. Dual-mode detection by PEC sensing and colorimetric sensing can achieve complementary advantages with high sensitivity, high selectivity, easy operation and visualisation. Comparatively, utilizing dual-mode detection can reduce external interference through different mechanisms and independent signal transduction pathways, and the detection results can be verified with each other, which has good feasibility and application prospects.

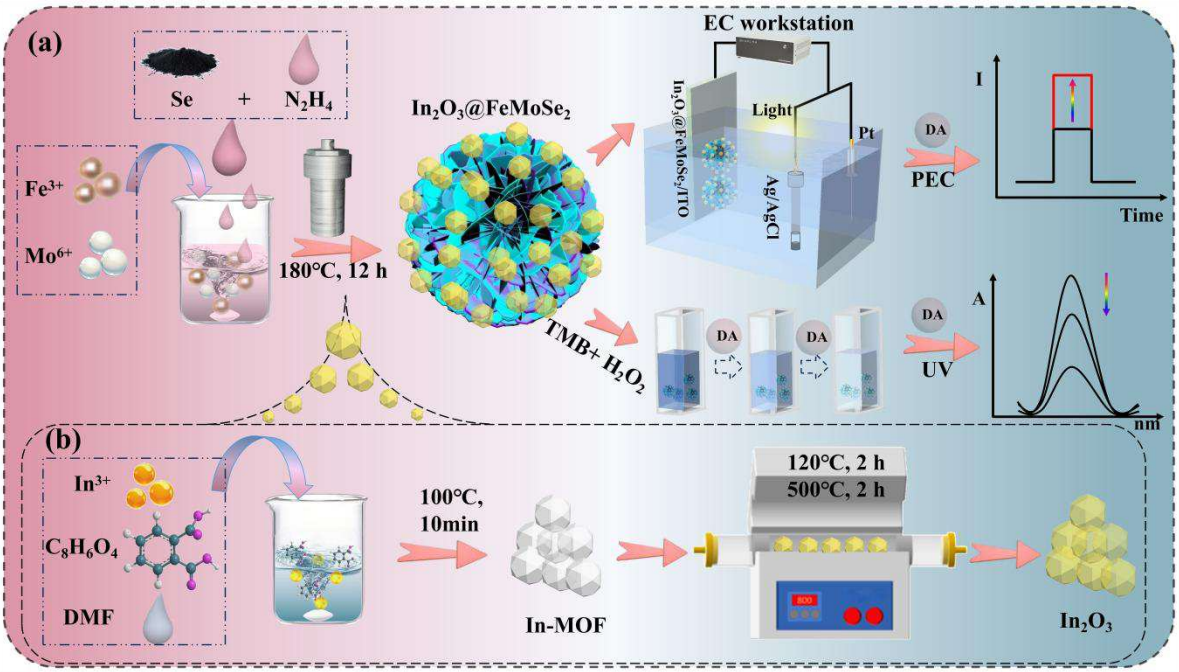
Indium oxide (In_2O_3) possessing a high specific surface area, which could be enhances the effective area for gas adsorption and desorption, thereby exhibiting excellent sensitivity. In_2O_3 exhibits a range of advantageous properties, including high mechanical stability and ease of surface functionalization, thanks to its surface electronic structure [14]. In addition, it is widely used as an active material in the field

of PEC sensors , gas sensors, transistors owing to these properties of good catalytic activity, permeability, adsorption, peroxide-like and wide bandgap[15-19]. For example, Xu et al. constructed an ultra-thin carbon nitride nanosheet-coated In_2O_3 with excellent properties. This novel architecture was specifically employed as a PEC sensor for monitoring diazinon (DZN) residues in water environments [20]. Functionalized In_2O_3 exhibits superior peroxidase-like activity, For instance, Ban et al. developed a straightforward yet highly sensitive sensor platform for hydrogen peroxide detection based on Ce doped IN peroxide-like materials [21].

Molybdenum diselenide ($MoSe_2$) is a novel semiconductor material with a unique electronic structure and high photoelectric conversion efficiency, which has attracted increasing attention as a photoactive material [22]. Owing to its large interlayer spacing, $MoSe_2$ readily allows the intercalation of metal ions such as Fe^{3+} and Li^+ to form intercalation compounds. This process modulates the electronic structure, increases the density of catalytically active sites, and enhances charge transfer conductivity and electrocatalytic activity. As a result, $MoSe_2$ holds broad applications in energy storage, oxygen reduction reaction (ORR) and the development of novel functional materials. Iron-doped molybdenum diselenide ($FeMoSe_2$) prepared by hydrothermal method exhibits a vertically aligned structure, which exposes more active edge sites and thereby enhances its electrocatalytic activity [23-24]. Although $FeMoSe_2$ with favourable electrical conductivity has been used as a sensitizer for electrochemical detection, it has been applied less in PEC sensing.

Herein, In_2O_3 nanoparticles with excellent mechanical stability, chemical

stability, and peroxidase-like activity were synthesized via the calcination of indium metal-organic frameworks (In-MOF). We have synthesized a novel In_2O_3@$FeMoSe_2$ heterojunctions for the first time leveraging the high electron mobility and excellent PEC performance of $FeMoSe_2$ and the high mechanical stability of In_2O_3. The overlap of bandgaps between the two monomers facilitates electron transfer, thereby enhancing the photoelectric conversion efficiency. The catechol structure of dopamine facilitates its role as an electron donor in charge transfer reactions. This electron donation process directly contributes to the amplification of the photoelectrochemical signal, enhancing detection sensitivity. Meanwhile, the peroxidase-like activity of the heterojunctions is enhanced, effectively catalyzing the conversion of hydrogen peroxide to hydroxyl radicals. Subsequently, these radicals mediate the oxidation of 3,3',5,5'-tetramethylbenzidine (TMB), generating a blue-colored derivative (TMBox) which exhibits a pronounced absorption maximum at 651 nm. DA reacts with hydroxyl radical and forms a competitive relationship with TMB, which indirectly inhibits the oxidation of TMB. The attenuation of the absorption peak, accompanied by a fading of the blue color, provided a straightforward visual method for dopamine (DA) detection. As depicted in Scheme 1, by taking advantage of two complementary detection methods to generate distinct signals, a colorimetric and PEC dual-mode sensing system based on In_2O_3@$FeMoSe_2$ heterojunctions was constructed, which was utilized to quantify DA with high sensitivity, stability, and wider linear range. This strategy further ensures the accuracy and reliability of the detection results.



Scheme 1. The preparation steps and detection schematic diagram of the dual-mode sensor.

2. Experimental

2.1. Reagents and apparatus

Dopamine hydrochloride (DA), indium nitrate hydrate ($In(NO_3)_3 \cdot xH_2O$), terephthalic acid ($C_8H_6O_4$), Ferric chloride hexahydrate ($FeCl_3 \cdot 6H_2O$) and selenium (Se) powder were purchased from Shanghai Alding Reagent Co., LTD. Hydrazine hydrate ($N_2H_4 \cdot xH_2O$) was purchased from Chengdu Kelon Chemical Reagent Factory. 0.2 M phosphate buffer solution (PBS) was prepared from NaH_2PO_4, Na_2HPO_4 and KCl.

The prepared materials were qualitatively analyzed using scanning electron microscopy (SEM, ZEISS Supra 55, Germany), X-ray photoelectron spectrometer (XPS, Thermo Fisher Scientific Co., Waltham, MA), transmission electron

microscopy (TEM, Philips Tecnai-12, Netherlands), and UV-Visible Spectrophotometer (UV-Vis, UV-1601, Shimadzu Corporation, Japan). The photoelectrochemical (PEC) response was measured using a CHI760e electrochemical workstation (Shanghai Chenhua Instrument Co., Ltd., China). An indium tin oxide (ITO) glass electrode, with a defined active area of 1 cm^2, served as the working electrode, platinum column electrode as the auxiliary electrode and Ag/AgCl electrode as the reference electrode. in a standard three-electrode configuration.

2.2. Synthesis of In_2O_3

In_2O_3 was prepared by hydrothermal synthesis [25]. First, 1 g of $C_8H_6O_4$ and 2.75 g of $In(NO_3)_3$-xH_2O were dispersed into 315 mL of DMF, and the reaction was carried out at 100 ℃ with continuous stirring for 10 min, The synthesized product was washed several times with anhydrous methanol and ethanol, followed by drying at 60 ° C, to yield the precursor In-MOF. The dried In-MOF was loaded into a tube furnace and thermal treatment in air at 120°C for 2 h. Subsequently, the temperature was elevated to 500°C at a controlled rate of 5°C/min and maintained at this temperature for 2 h to ensure complete conversion to the desired metal oxide phase. Cool the product to room temperature to obtain pale yellow In_2O_3 powder.

2.3. Synthesis of In_2O_3@$FeMoSe_2$ heterojunctions

In_2O_3@$FeMoSe_2$ heterojunctions were synthesised improved method. 0.2 g of $FeCl_3$ $6H_2O$ and 0.2 g of Na_2MoO_4-$2H_2O$ dissolved into 20 mL of deionised water to prepare a mixed solution A. 0.12 g of selenium powder was dissolved in 10 mL of hydrazine hydrate (N_2H_4-xH_2O) to prepare a mixed solution B, followed by slowly

added dropwise to solution A, and heated at 180 °C for 12 h. Finally, the In_2O_3@$FeMoSe_2$ heterojunctions were obtained by centrifugation, washed with ethanol and deionised water, and then dried under vacuum at 60 °C. $FeMoSe_2$ was synthesized by the same method, except that In_2O_3 was not added.

2.4. Preparation of modified electrodes

The ITO (5×1 cm, <6 Ω) conductive glass electrode was successively cleaned with acetone and anhydrous ethanol by ultrasonication for 20 min, and then cleaned by ultrasonication with deionised water and then dried with infrared lamp for spare. 1 mg of In_2O_3@$FeMoSe_2$ heterojunctions were ultrasonically dispersed in 1 mL of deionised water to make 1 mg/mL In_2O_3@$FeMoSe_2$ suspension. Accurately aspirate 10 μL of the suspension to coat the conductive surface of the ITO glasselectrode, and dry naturally to obtain In_2O_3@$FeMoSe_2$/ITO. 1 mg/mL of In_2O_3 suspension and 1 mg/mL of $FeMoSe_2$ suspension were prepared by the same method, and In_2O_3/ITO and $FeMoSe_2$/ITO were produced.

2.5. Analytical performance of dual-mode detection DA

The PEC properties of the modified ITO electrodes were investigated using the time-current method (i-t) and electrochemical impedance spectroscopy (EIS). i-t parameters were set to an initial potential of 0 V and a sampling interval of 0.5 s. EIS measurement was configured with a bias potential of 0.35 V, an AC amplitude of 0.005 V, and a frequency sweep ranging from 10^4 Hz to 1 Hz, preceded by a 2 s settling time at each frequency. The peroxidase activity of the prepared peroxidase-like material (In_2O_3@$FeMoSe_2$) was detected by colorimetric method

using a UV-visible spectrophotometer, and the substrate was prepared as follows. 0.2 mL of TMB (0.05 M), 0.2 mL of H_2O_2 (0.2 M), and 0.1 mL of an aqueous dispersion of In_2O_3@$FeMoSe_2$ (1 mg/mL) were added to 1.5 mL of PBS buffer solution (0.1 M, pH 4.0), respectively. A series of different concentrations of DA were introduced to the substrate, followed by a subsequent incubation period of 30 min at room temperature. Finally, the supernatants were obtained by centrifugation, and then detected the UV-visible spectrophotometry.

3. Results and discussion

3.1. Characterizations of the materials

The morphological and structural features of In_2O_3 and In_2O_3@$FeMoSe_2$ heterojunctions were estimated by scanning electron microscope (SEM). As Fig. 1A and 1B, the In_2O_3 exhibits uniform nanoparticles. In the case of In_2O_3@$FeMoSe_2$ hybrid, displays a uniform three-dimensional architecture composed of micro-flowers that are assembled from numerous interconnected, petal-like nanosheets. These uniform nanosheets provide a large specific surface area and a large number of active sites for enhancing effective PEC catalysis. SEM images of In_2O_3@$FeMoSe_2$ heterojunctions reveal that the $FeMoSe_2$ microflowers are uniformly decorated with In_2O_3 nanoparticles, forming a well-integrated heterojunction structure that facilitates efficient charge transfer (Fig. 1C and 1D). The morphology and microstructure of the flower-like In_2O_3@$FeMoSe_2$ heterojunctions is characterized by transmission electron microscope (TEM). The In_2O_3 expresses ellipsoidal nanospheres with a size of about 30 nm, and $FeMoSe_2$ shows a sheet like morphology (Fig. 1E and 1F).

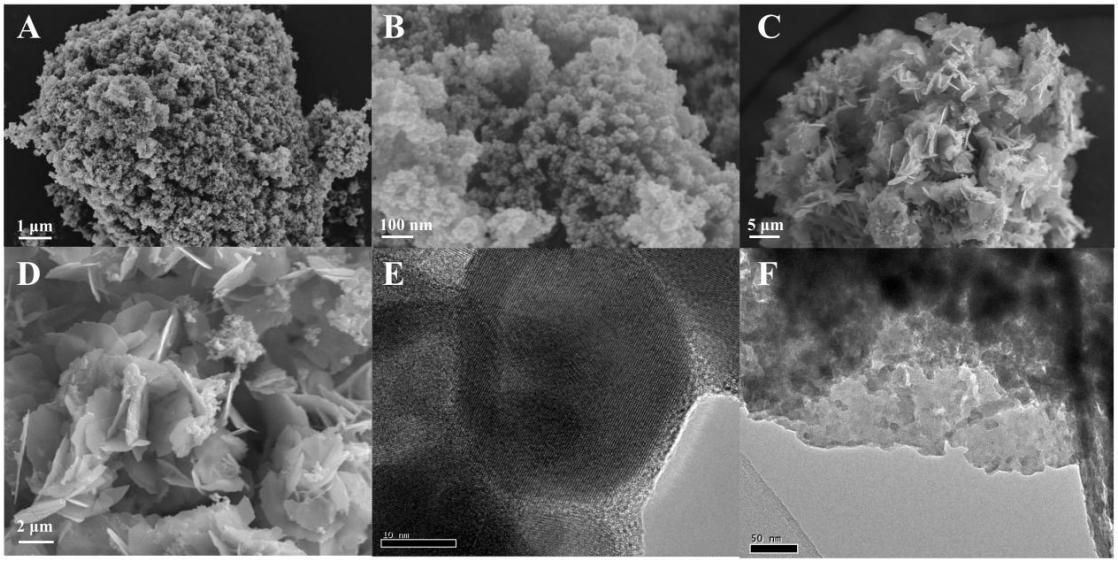


Fig. 1 (A) and (B) are SEM images of In_2O_3, (C) and (D) are SEM images of In_2O_3@$FeMoSe_2$, (E) and (F) are TEM images of In_2O_3@$FeMoSe_2$

The chemical bonding, binding energies and valence states of In_2O_3@$FeMoSe_2$ heterojunctions were evaluated through X-ray photoelectron spectroscopy (XPS). The full scan XPS spectrum shows the peaks of O, Mo, Fe, In and Se elements (Fig. 2A). In the high-resolution scan of O 1s, the spectral peaks at 529.4 eV and 531.1 eV correspond to the two different chemical states of lattice oxygen (OL) and oxygen vacancy (OV) of the In-O bond, respectively (Fig. 2B) [26]. The peaks appear at of Mo 3d assigned to 229.2 eV, 231.7 eV and 232.5 eV, 234.7 eV exhibit two mixed valence states of Mo^{6+} and Mo^{2+}, respectively (Fig. 2C). The characteristic peaks at 710.7 eV and 724.6 eV belong to Fe $2p_{3/2}$ and Fe $2p_{1/2}$, reflecting the presence of Fe^{3+} species (Fig. 3D). The peaks located at 444.0 eV and 451.6 eV are are ascribed to the two electronic states of In^{3+} 3d $_{3/2}$ and In^{3+} $3d_{5/2}$, respectively (Fig. 2E). The Se 3d section can be separated into two obvious peaks at 53.9 eV and 54.9 eV, corresponding to Se $3d_{3/2}$ and Se $3d_{5/2}$, respectively (Fig. 3F) [27].

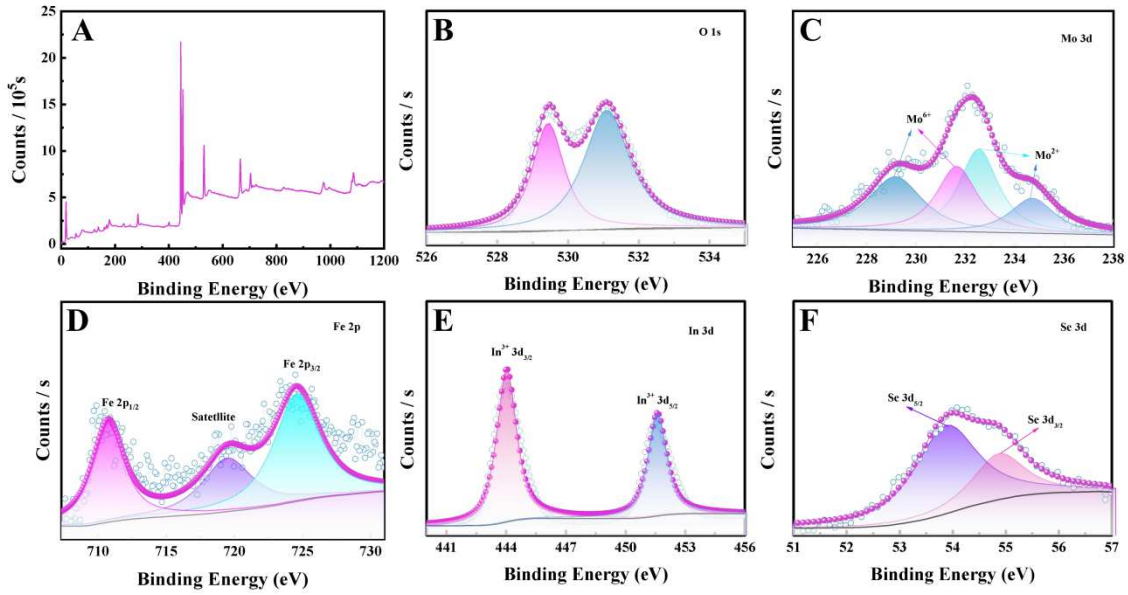


Fig. 2 XPS analysis of In_2O_3@$FeMoSe_2$ (A), high-resolution XPS spectra of (B) O 1s, (C) Mo 3d, (D) Fe 2p, (E) In 3d, (F) Se 3d

It is well known that the energy band structure is affected by the charge transfer at the interface of the composite junction. In the work, the UV-Vis diffuse reflectance spectra (DRS) was employed to monitor the light absorption properties of the prepared PEC materials. As Fig. 3A, the bandgap energy (E_g) value was calculated by the following Tauc equation[28]:

$$(\alpha h\nu)=K(h\nu-E_g)^n \qquad (1)$$

where α, h, ν, K, E_g, refer to the absorption coefficient, Planck's constant, frequency of light, forbidden bandwidth of the semiconductor, respectively. $h\nu$ denotes the energy of the photon, and n *is* directly related to the type of semiconductor. The n value of direct bandgap semiconductors is 1/2. In the case of direct bandgap semiconductors, n value is 1/2. The n values of 1/2 for both In_2O_3 and $FeMoSe_2$ are attributed to the fact that they are direct bandgap semiconductors. By converting DRS

to the graph shown in Fig.3B based on the Tauc equation, the E_g values of In_2O_3, $FeMoSe_2$ and In_2O_3@$FeMoSe_2$ are 3.58 eV, 1.75 eV and 2.13 eV for, respectively [29-30]. The Eg value of the heterojunctions is reduced by 1.45 eV after bonding with $FeMoSe_2$ compared to In_2O_3. Besides, the types of semiconductors were investigated by Mott-Schottky (M-S) analyses, as shown in Fig. 3C and 3E. The results show that the M-S curves of In_2O_3 and $FeMoSe_2$ are positive tangent slopes, demonstrating that they are typical n-type semiconductors. The extrapolated CB positions of In_2O_3 and $FeMoSe_2$ are -2.10 eV, and -0.08 eV (vs. NHE), respectively, attribute to the flat bands of n-type semiconductors are closer to their conduction band (CB) positions. By analyzing the *M-S* curves, the intercepts correspond to -2.30 eV and -0.28 eV, respectively (vs. NHE). The order band (VB) positions of In_2O_3 and $FeMoSe_2$ are calculated to be 1.48 eV and 1.67 eV, respectively, based on the Eg values.

Fig. 3F briefly illustrates the proposed interfacial electron transfer mechanism of the In_2O_3@$FeMoSe_2$ heterojunctions. The effective hybrid of In_2O_3 and $FeMoSe_2$ promotes the separation of electrons and photovoltaic holes at the binary heterojunction interface. Plainly, under light irradiation, In_2O_3 and $FeMoSe_2$ exhibit complementary and matching light absorption energies. The established hybrid band structure subsequently facilitated the efficient migration of photogenerated electrons (e^-) from the conduction band (CB) of In_2O_3 to that of $FeMoSe_2$. Meanwhile, holes (h^+) are transferred from $FeMoSe_2$ with higher VB to In_2O_3 with lower VB. This energy band structure promotes the spontaneous transfer of electrons from high energy level to low energy level, thus reducing the possibility of recombination of e^- and h^+, and

improving the efficiency of photoelectric conversion. As an electron donor, DA promotes the separation of e^--h^+ and enhances the optical signal. DA acts as an effective electron donor, readily suppressing charge carrier recombination by transferring e^- to trap h^+. This process effectively enhances the PEC response. The specific equation can be represented as follows:

$$In_2O_3@FeMoSe_2 + h\nu \rightarrow h^+ + e^- \quad (2)$$

$$h^+ + DA \rightarrow 5,6\text{-Dihydroxyindole } (DA^+) \quad (3)$$

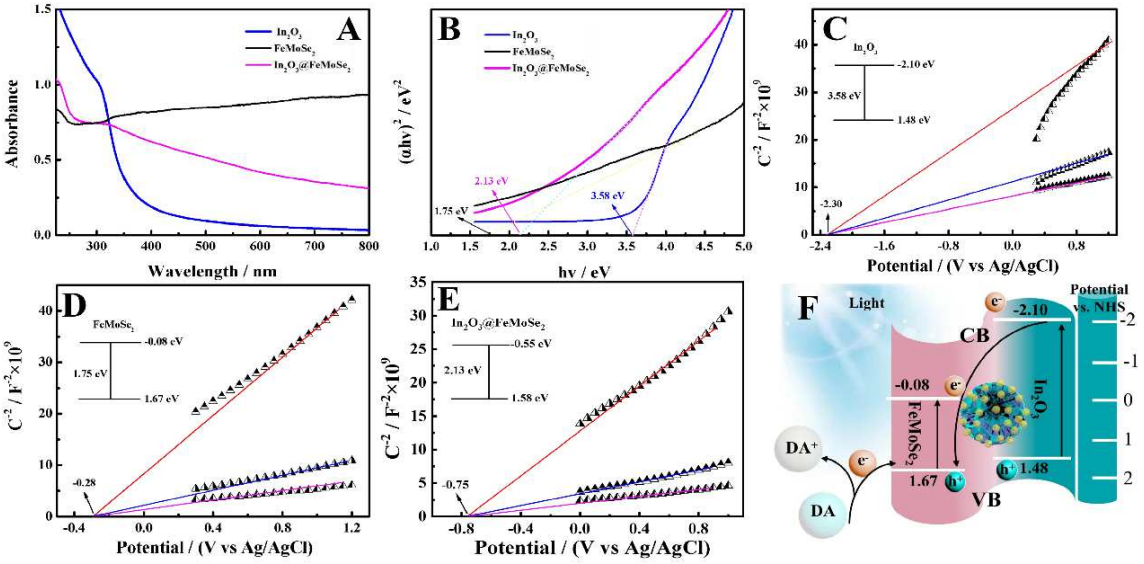


Fig. 3 (A) Tauc evaluation of band-gap energy of different materials; Mott-Schottky curves for (B) In_2O_3, (C) $FeMoSe_2$ and (D) In_2O_3@$FeMoSe_2$. (F) The photoelectron transfer mechanism of the In_2O_3@$FeMoSe_2$/ITO in the presence of DA

3.2. Feasibility of the ternary In_2O_3@$FeMoSe_2$ based sensor

The feasibility of the In_2O_3@$FeMoSe_2$ based sensor was investigated by recording its PEC signals and absorbance (Fig. 4A). The photoelectric conversion efficiencies of different materials modified electrodes in 0.2 M PBS buffer solution (pH 7.0) were explored, there was almost no photocurrent in bare/ITO and In_2O_3/ITO.

The PEC current values of $FeMoSe_2$/ITO and In_2O_3@$FeMoSe_2$/ITO are 63.2 nA, 100.8 nA, respectively. The In_2O_3@$FeMoSe_2$/ITO exhibit highest photocurrent than the monolithic electrodes, indicating the higher photoelectric conversion efficiency. For comparison, the photocurrent of In_2O_3@$FeMoSe_2$/ITO increases to 278.6 nA in the presence of 47.8 μM DA (Fig. 4B). The result shows that In_2O_3@$FeMoSe_2$ has a certain degree of strong catalytic activity towards DA, and the photocurrent changes by 2.8 times in the absence and presence of DA. Meanwhile, Electrochemical impedance spectroscopy (EIS) technology was used to analyze the ability of electron transfer in 5 mM $[Fe(CN)_6]^{3-/4-}$ containing 0.1 M KCl for these materials modified electrodes (Fig. 4C). Obviously, the electron transfer resistance (Ret) of $FeMoSe_2$/ITO is smaller than bare/ITO, owing to the excellent conductivity that seriously increases the electron transfer rate. The Ret value is the smallest on the In_2O_3@$FeMoSe_2$/ITO, thanks to good synergistic effect, and implies successfully hybrid.

To investigate the peroxidase-like properties of different materials, the catalytic oxidation of the chromogenic substrate TMB was analyzed both in the presence and absence of H_2O_2 (Fig. 4D and 4E). In the absence of H_2O_2 presence, the reaction system containing TMB and In_2O_3@$FeMoSe_2$ (curve a) shows non-significant UV absorption, indicating that In_2O_3@$FeMoSe_2$ is a peroxidase-like enzyme material. In contrast, all three systems containing only H_2O_2 (curve b), In_2O_3 and H_2O_2 (curve c) and $FeMoSe_2$ (curve d) had low absorption, suggesting that H_2O_2 alone or with the monomer triggers the oxidation of TMB only slightly. When TMB, H_2O_2 and In_2O_3@$FeMoSe_2$ are present simultaneously, a stronger absorption intensity can be

observed, accompanied by a marked darkening of the blue color. The absorption strength of In_2O_3@$FeMoSe_2$ is 1.7 times and 2.0 times higher than that of In_2O_3 and $FeMoSe_2$, respectively. These results indicate In_2O_3@$FeMoSe_2$ has an excellent peroxidase-like activity.

3.3 Optimisation of experimental conditions

In the process of constructing the PEC sensor, the concentration of the In_2O_3@$FeMoSe_2$ suspension was rigorously optimized. Blue light (20 W) was used as the excitation light source, and the potential was set to 0 V. As illustrated in Fig. 4F and 4G, the relative photocurrent increment, denoted as $_{\Delta}I$, was defined as the absolute difference in photocurrent between the target sample (I) and the blank reference (I_0), calculated using the formula $_{\Delta}I = |I-I_0|$. $_{\Delta}I$ was positively correlated with the In_2O_3@$FeMoSe_2$ concentration, showing more photogenerated electrons, and reached its maximum value when the concentration was 5 mg/mL. Therefore, the concentration at 5 mg/mL of In_2O_3@$FeMoSe_2$ suspension was selected as the optimal value for all subsequent of the PEC sensor. In addition, photocurrent response of In_2O_3@$FeMoSe_2$/ITO in PBS buffer containing 47.8 μM DA at different pH was investigated (Fig. 4H and 4I). $_{\Delta}I$ reached the maximum value at pH 7.0. Hence, the PBS buffer solution with pH 7.0 was chosen as the optimal pH condition in PEC sensing.

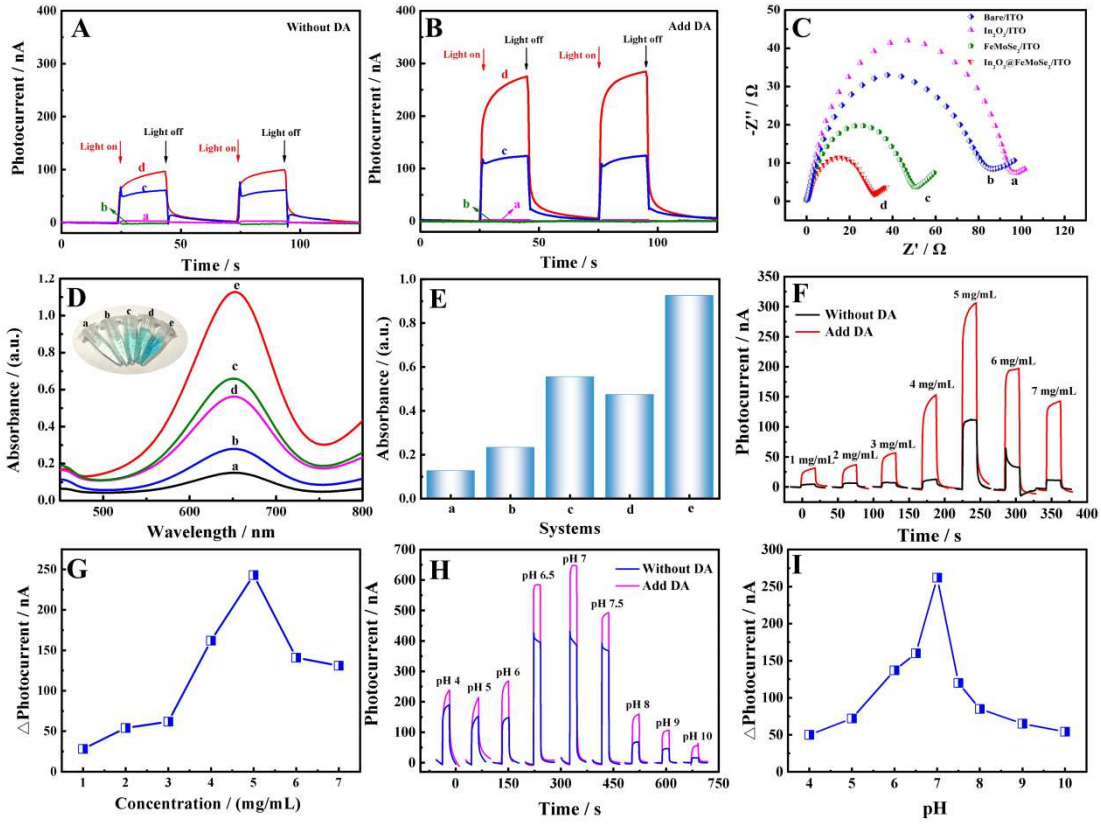


Fig. 4 Photoelectric curves of different modified electrodes (A) without DA, (B) with DA (C) EIS diagram of different modified electrodes; (C) UV-VIS absorption spectra of various reaction systems: (a) TMB+In_2O_3@$FeMoSe_2$, (b) TMB+H_2O_2, (c) TMB+H_2O_2+In_2O_3, (D) TMB+H_2O_2+$FeMoSe_2$, (e)TMB+H_2O_2+In_2O_3@$FeMoSe_2$ and (D) absorbance of each reaction system; (F) Diagram of the influence of the modified electrode with different In_2O_3@$FeMoSe_2$ concentrations on the photocurrent response and (G) corresponding data; (H) Influence graphs of photocurrent response of In_2O_3@$FeMoSe_2$/ITO at different pH and (I) corresponding data

3.4. Analysis of DA

The quantitative performance of the sensor base on In_2O_3@$FeMoSe_2$ heterojunctions was investigated. It is show that the photocurrents exhibit gradual increase with the DA concentrations using the time-current (i-t) method under optimal

experimental conditions (Fig. 5A). As further evidence, the photocurrents reveal linear dependence with the DA concentrations in a range from 0.05 to 100 μM, with a linear regression equation of I(nA)=3.34C(μM)+105.76 (R=0.9982) (Fig. 5B). The detection limit (LOD) is calculated to be 14.7 nM. Meanwhile, it is found that the absorbance of exhibit gradual reduction and the blue color of the reaction solution gradual becoming lighter with the DA concentrations in a range from 0.5 to 75 μM using UV-Vis spectrophotometry at 651 nm (Fig. 5C), with a linear regression equation of A=-0.0123C(μM)+1.07 (R=0.9970) (Fig. 5D). The LOD is calculated to be 0.19 μM. The analytical performance of the developed sensor was rigorously compared with the previously established methods for DA detection (Table.1), indicated that the wider linear range and lower LOD of the PEC and colorimetric sensor based on In_2O_3@$FeMoSe_2$ heterojunctions can achieve dual-mode detection.

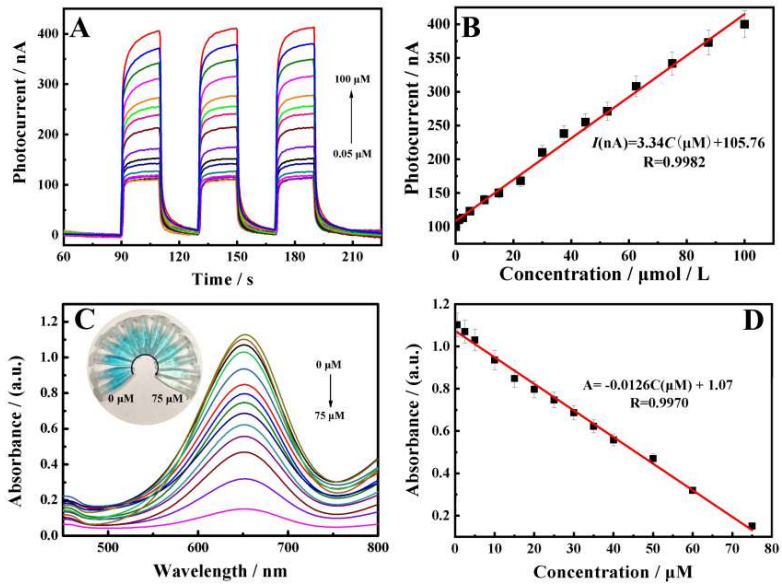


Fig. 5 (A) Photocurrent curves of different concentrations of DA (0.05-100 μM) and (B)its standard curves; (C) UV-VIS spectra of DA (0-75 μM) at different concentrations and (D) its standard curves.

Table.1 Comparison of other methods for the determination of DA

Materials/Electrodes	Methods	Linear range (μM)	LOD (μM)	Refs.
$ZnIn_2S_4/TiO_2/FTO$	PEC	0.5–1000	0.253	[5]
ZnMOF/ITO/FTO	PEC	0.03-10	0.0177	[6]
$(001)TiO_2/Ti_3C_2$	PEC	1-1000	0.52	[31]
$CsPb_2Br_5/CdS$	PEC	0.3 – 300	0.0116	[32]
AuMS	colorimetric	10.0-80.0	128	[33]
MoS_2/graphene	colorimetric	1-400	0.21	[34]
$CoFe_2O_4$	colorimetric	5–80 μM	0.233	[35]
In_2O_3@$FeMoSe_2$/ITO	PEC	0.05-100	0.0147	This work
	colorimetric	0.5-75	0.19	

3.5 Selectivity and stability

It is acknowledged that actual samples frequently exhibit complicated compositions, thus necessitating high selectivity to guarantee the analytical performance and usefulness of the dual-modal platform. Therefore, the sensor was investigated with some typical possible interferences such as cations (Ca^{2+}, Mg^{2+}, Na^{+}, and K^{+}), uric acid (UA), L-cysteine (Cys), ascorbic acid (AA), glucose (Glu), glycine (Gly), arginine (Arg), and glutathione (GSH) in the presence of DA, and the possible interferences concentrations equivalent to 50 times DA. The effects of DA alone and possible interferences co-existence in the PEC and colourimetric sensing tests were shown in Figs. 6A and 6B, respectively. A negligible variation is observed in the presence of such interferences by comparing the relative activity, indicating that the

proposed bimodal sensor has good selectivity. Besides, the stability of the PEC in the absence and presence of 30 μM DA was investigated with RSDs of 0.33% and 0.74%, respectively, indicating a high stability (Fig. 6C).

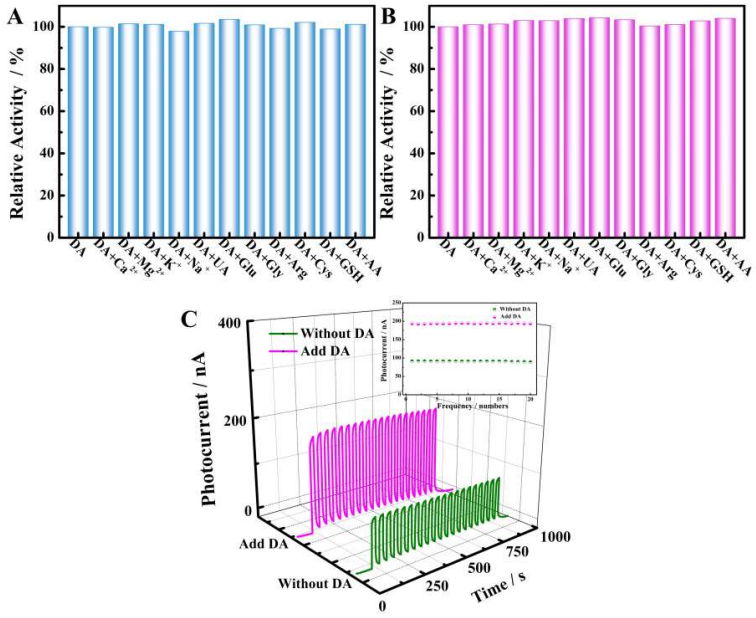


Fig. 6 (A) Photocurrent ratio diagram and (B) absorbance ratio diagram of DA and interferors alone and co-existing; (C) short-term stability in In_2O_3@$FeMoSe_2$ systems with and without DA (inset: corresponding data)

3.6. Real sample analysis

The practicability and application prospect of the dual-modal system were subjected to evaluation by standard addition method. This was achieved by introducing precise volumes of DA standard stock solutions into aliquots of the human serum and urine samples to generate a concentration gradient for accurate quantification. The samples were determined by recovery based on PEC and colorimetric sensor successively, and the results are shown in Table 2. The recoveries of DA were 101.30%~102.7% and 95.88%~98.48%, respectively, and the RSDs

ranging from 1.56% to 3.51% and 1.88% to 3.10%, respectively. The results show that the dual-modal system is reliable and can be used for the determination of dopamine in biological samples.

Table.2 Detection results for DA in human serum and urine samples (N=3)

Samples	Added (μM)	PEC sensor			Colorimetric sensor		
		Found (μM)	Recovery (%)	RSD (%)	Found (μM)	Recovery (%)	RSD (%)
Human serum	5	5.10	102.00	1.25	4.89	95.88	2.78
	10	10.13	101.30	2.34	9.87	96.76	3.10
	60	60.82	101.37	3.51	59.10	97.17	2.58
Human urine	5	5.07	101.40	2.32	4.89	97.44	1.90
	10	10.27	102.70	1.56	9.91	97.92	2.12
	60	60.48	100.80	2.78	59.56	98.48	1.88

4. Conclusion

In summary, a novel In_2O_3@$FeMoSe_2$ heterojunctions were prepared synthesized with a cost-effective hydrothermal method. The material exhibited excellent photoelectrocatalytic activity, peroxidase activity and stability, which successfully designed and constructed to the PEC and colorimetric dual-mode sensor for sensitive analysis of DA. The dual-mode sensor exhibits excellent stability and sensitivity, as well as a low detection limit. It is suitable for the detection of DA in human serum and urine for practical applications, and is a versatile, high-performance, economical and convenient dual-mode detection platform. Consequently, this efficient sensing

strategy has considerable potential and broad prospects in biological research.

Conflict of interest The authors declare that they have no known competing financial interests or personal relationships that could have appeared to influence the work reported in this paper.

Acknowledgements We would like to acknowledge the Scientific Innovation Teams of Guangxi Minzu Normal University (Grant No. KYTD202405) and the Chongzuo City Science and Technology Project (Grant No. 2026ZC0503) and the Universities in Guangxi Young and Middle-Aged Teachers' Basic Ability Improvement Project (Grant No. 2024KY0784).

Author contributions Qing Huang: Writing-review and editing; Funding acquisition; Data curation; Supervision; Writing-original draft; Conceptualization. Ju Huang: Writing-review and editing; Methodology. Lei Huang: Methodology; Resources; Supervision. Tao Yang: Resources; Supervision. Yanli Zhang: Methodology; Resources; Supervision. Chendong Ling: Resources; Investigation. Cuizhong Zhang: Investigation; Resources. Wen-feng Zhuge: Resources; Supervision; Writing-review and editing; Funding acquisition. Jinyun Peng: Validation; Methodology; Funding acquisition; Writing-review and editing. Qiaoqiao Sun: Methodology; Resources; Supervision.

Funding This work was supported through by the Scientific Innovation Teams of Guangxi Minzu Normal University (Grant No. KYTD202405) and the Chongzuo City Science and Technology Project (Grant No. 2026ZC0503) and the Universities in

Guangxi Young and Middle-Aged Teachers' Basic Ability Improvement Project (Grant No. 2024KY0784).

Data availability No datasets were generated or analysed during the current study.

Generative AI and AI-assisted technologies During the preparation of this work, the authors did not use any generative AI or AI-assisted technologies in the writing, preparation, generation, modification, or enhancement of the manuscript, figures, or graphical abstract.

References

[1] Inagaki H, de-Leon S, Wong A, Jagadish S, Ishimoto H, Barnea G, Kitamoto T, Axel R, Anderson D (2012) Visualizing neuromodulation in Vivo: TANGO-mapping of dopamine signaling reveals appetite control of sugar sensing. Cell 148:583-595. https://doi.org/10.1016/j.cell.2011.12.022

[2] Li Z, Zhang H, Zha Q, Zhai C, Li W, Zeng L, Zhu M (2020) Zeng, M. Zhu. Photo-electrochemical detection of dopamine in human urine and calf serum based on MIL-101(Cr)/carbon black. Microchim Acta 187(9):526. https://doi.org/10.1007/s00604-020-04524-z

[3] Fuente-Fernández R, Ruth T, Sossi V, Schulzer M, Calne D, Stoess A (2001) Expectation and dopamine release: mechanism of the placebo effect in parkinson's disease. Sci 293(5532):1164-1166. https://doi.org/10.1126/SCIENCE.1060937

[4] Hoang H, Matsumoto N, Miyano M, Ikegaya Y, Cortes A (2025) Dopamine-induced relaxation of spike synchrony diversifies burst patterns in

cultured hippocampal networks. Neural Networks 181:106888. https://doi.org/10.1016/j.neunet.2024.106888

[5] Shen M, Hu X (2025) A "signal-off" anodic photoelectrochemical sensor based on $ZnIn_2S_4/TiO_2$ heterojunction for dopamine detection. Talanta 281:126800. https://doi.org/10.1016/j.talanta.2024.126800

[6] Kong W, Zhu D, Luo R, Yu S, Ju H (2022) Framework-promoted charge transfer for highly selective photoelectrochemical biosensing of dopamine. Biosens Bioelectron 211:114369. https://doi.org/10.1016/j.bios.2022.114369

[7] Treepet S, Duangmanee T, Chokradjaroen C, Kim K, Saito N, Watthanaphanit A (2025) Solution plasma synthesis of nitrogen-doped carbon dots from glucosamines: Comparative fluorescence modulation for dopamine detection. Carbon 231:119705. https://doi.org/10.1016/j.carbon.2024.119705

[8] Xu Y, Zhou J, Sun P, Li P, Han D, Wang X, Chai F (2025) The construction of peroxidase-like Cu-BDC@$FeMo_6$ for colorimetric detection of H_2O_2 and dopamine. Sep Purif Technol 353:128396. https://doi.org/10.1016/j.seppur.2024.128396

[9] Wang Y, Kang K, Wang S, Ma L, Kang W, Liu XH, Niu LM, Guo Z (2020) A novel resonance rayleigh scattering aptasensor for dopamine detection based on an exonuclease III assisted signal amplification by g-quadruplex nanowires formation. Arabian J Chem 13(8):6598-6605. https://doi.org/10.1016/j.arabjc.2020.06.016

[10] Wang H, Dong L, Zhao L, Sun Y, Zhang R, Shan G (2025) Portable paper-based microfluidic devices based on CuS@Ag_2S nanocomposites for colorimetric/electrochemical dual-mode detection of dopamine. Biosens Bioelectron 273:117162. https://doi.org/10.1016/j.bios.2025.117162

[11] Dashtian K, Hajati S, Ghaedi M (2022) Molecular imprinted poly(2,5-benzimidazole)-modified VO_2-$CuWO_4$ homotype heterojunction for photoelectrochemical dopamine sensing. Anal Chem 94(18):6781-6790. https://doi.org/10.1021/acs.analchem.2c00485

[12] Liu F, Huang W, Wu G, Zhang Z, Xiang G, Huang Y, Pan Z, Peng J (2026) Dual enzyme-mimicking Ce-UiO-66-NO_2-driven autocatalytic cascade signal amplification for split-type electrochemical aptasensing of enrofloxacin. Food Chem 517:149502 . https://doi.org/10.1016/j.foodchem.2026.149502

[13] Woo S, Kim H, Youn P, Lee K, Kang G, You S, Lee K, Kim Y, Yu S, Han J, Yoo S, Park I (2025) Reactive metal-support interaction of In_2O_3/crystalline carbon hybrid support for highly durable and efficient oxygen reduction reaction electrocatalyst. Chem. Eng J 505:159586. https://doi.org/10.1016/j.cej.2025.159586

[14] Zheng Y, Sun P, Liu S, Nie W, Bao H, Men L, Li Q, Su Z, Wan Y, Xia C, Xie H (2025) Solar energy powered electrochemical reduction of CO_2 on In_2O_3 nanosheets with high energy conversion efficiency at a large current density. J Colloid Interface Sci 678:722-731. https://doi.org/10.1016/j.jcis.2024.08.177

[15] Zhu L, Zhao H, Wang S, Li C, Jing L, Liu K, Xie L, Ge S, Yu J (2026) Ternary In_2O_3/$ZnIn_2S_4$/CdS heterojunction-based APE1-assisted “AND” logic gate photoelectrochemical biosensor for dual-miRNA detection. Anal Chim Acta 142:3346194. https://doi.org/10.1016/j.aca.2026.346194

[16] Liu X, Jia C, Zhang J, Zhou Y, Wang S, Luo J, Li X, Wang Y, Guo C(2026) Constructing Co_3O_4/In_2O_3 heterojunction hollow hexagonal prisms for acetone gas sensors with ultra-high response and low operating temperature. Sens Actuators B Chem 467:140537. https://doi.org/10.1016/j.snb.2026.140537

[17] Yang W, Huo Y, Wang T, Liu X, Li D, Yu H, Dong X, Yang Y (2025) RGO@In_2O_3 based flexible gas sensor: Efficient monitoring of trace NO_2 gas at room temperature. Sens Actuators B Chem 430:137359. https://doi.org/10.1016/j.snb.2025.137359

[18] Zhang H, Wang Y, Chen X, Zhang K, Li D, Tong Y, Ling J, Zhang M (2026) Dual-gas sensor based on $CdIn_2O_4/In_2O_3$ heterostructure nanofiber arrays for trace detection of n-butanol and formaldehyde. Sens Actuators B Chem 468:140764. https://doi.org/10.1016/j.snb.2026.140764.

[19] Yeom G, Park J, Park M, Hwang J, Lee J (2025) Novel floating-gate structure of In_2O_3 thin-film transistor-based gas sensor for improved gas sensing properties. Sens Actuators B Chem 426:137046. https://doi.org/10.1016/j.snb.2024.137046

[20] Yan P, Huang J, Wu G, Zhang Y, Mo Z, Xu K, Ling M, Dong S, Xu L, Li H (2025) Construction of a In_2O_3/ultrathin g-C_3N_4 S-scheme heterojunction for sensitive photoelectrochemical aptasensing of diazinon. J Colloid Interface Sci 679:653-661. https://doi.org/10.1016/j.jcis.2024.10.016

[21] Liu B, Ruan H, Li C, Yao J, Wei B, Wang L, Ban S, Xie J (2023) Ce-doped indium oxide nanozymes with peroxidase-like activity induced by cerium–indium synergy for colourimetric detection of H_2O_2. New J Chem 47(39):18476-18484. https://doi.org/10.1039/D3NJ02985A

[22] Singh P, Devi P (2024) Deciphering the photoelectrochemical behaviour of $MoSe_2$-decorated $BiVO_4$ as a dual system for concurrent degradation of methylene blue and hydrogen generation. J Cleaner Prod 448:141502. https://doi.org/10.1016/j.jclepro.2024.141502

[23] Jiang S, Zhang L, Yu H, Deng K, Wang Z, Xu Y, Wang H, Wang L (2024) Heterostructure and interface engineering of $Ni_{0.85}Se$-$MoSe_2$@PEI for enhancing

electrocatalytic acidic oxygen reduction to hydrogen peroxide. Chem Eng J 489: 151272. https://doi.org/10.1016/j.cej.2024.151272

[24] Lin Z, Fu B, An Y (2020) An. Effects of defects and anions on the geometry, electronic structures and exchange interaction of Fe-doped 2H-$MoSe_2$ monolayer. Appl Surf Sci 528:146960. https://doi.org/10.1016/j.apsusc.2020.146960

[25] Cho W, Lee HJ, Oh M (2008) Growth-controlled formation of porous coordination polymer particles. J Am Chem Soc 130(50):16943-16946. https://doi.org/10.1021/ja8039794

[26] Xiong S, He S, Wu L, Zhao H, Liu C (2026) Oxygen vacancy induced strong interaction of single atom Ru with In_2O_3 for improved CO_2 hydrogenation to methanol. Chem Eng J 529:172660. https://doi.org/10.1016/j.cej.2026.172660

[27] Kaur R, Singh K, Tripathi S (2020) Tripathi. Study of linear and non-linear optical responses of $MoSe_2$-PMMA nanocomposites. J Mater Sci:Mater Electron 31(22):1-15. https://doi.org/10.1007/s10854-020-04520-2

[28] Li L, Xie Y, Luo C, Pen G, Min Z, Huang X, Fu R, Gao Y, Wang Z, Lu L (2025) Highly efficient Z-scheme CeO_2/Bi_2MoO_6 heterojunction strengthened by redox mediator for photoelectrochemical detection of tetracycline with enhanced sensitivity. Food Chem 465:141893. https://doi.org/10.1016/j.foodchem.2024.141893

[29] Shah S, Hussain S, Din S, Shahid A, Amu-Darko J, Wang M, You T, Liu G, Qiao G (2024) A review on In_2O_3 nanostructures for gas sensing applications. J Environ Chem Eng 12(3):112538. https://doi.org/10.1016/j.jece.2024.112538

[30] Tian M, Gao Y, Zhang Y, Ren M, Lv X, Hou K, Jin C, Zhang H, Lian R, Gong P, Wang R, Wang J, Shi X (2024) Toward direct band gaps in typical 2d

transition-metal dichalcogenides junctions via real and energy spaces tuning. Commun Mater 5(1):1-9. https://doi.org/10.1038/s43246-024-00631-z

[31] Chen Y, Li X, Cai G, Li M, Tang D (2021) Tang. In situ formation of (001) TiO_2/Ti_3C_2 heterojunctions for enhanced photoelectrochemical detection of dopamine. Electrochem Commun 125:106987. https://doi.org/10.1016/j.elecom.2021.106987

[32] Zheng Y, Zhao G, Liu S, Guo Y, Liu B, Lu W, Tao Z, Song C, Liu J, Li R, Huang M (2026) All-inorganic perovskite $CsPb_2Br_5$/CdS heterojunction for photoelectrochemical dopamine detection. Chem Eng J 543:178480. https://doi.org/10.1016/j.cej.2026.178480

[33] Ray S, Biswas R, Banerjee R, Biswas P (2020) A gold nanoparticle-intercalated mesoporous silica-based nanozyme for the selective colorimetric detection of dopamine. Nanoscale Adv 2(2):2734-745. https://doi.org/10.1039/C9NA00508K

[34] Lv Q, Chen L, Liu H, Zou L (2022) Peony-like 3D-MoS_2/graphene nanostructures with enhanced mimic peroxidase performance for colorimetric determination of dopamine. Talanta 247:123553. https://doi.org/10.1016/j.talanta.2022.123553

[35] Sun P, Chen J, Li Q, Luo M, Chang W, Xue Z (2025) Self-signaling colorimetric sensor for selective detection of dopamine based on $CoFe_2O_4$ nanozyme accelerated dopamine polymerization. Anal Chim Acta 1338(8):343596. https://doi.org/10.1016/j.aca.2024.343596

Supplementary Files

This is a list of supplementary files associated with this preprint. Click to download.

- GraphicalAbstract.tif